Ocean Dynamics (2014) 64:459–469
DOI 10.1007/s10236-014-0694-9

Variations of tidally driven three-layer residual circulation in fjords

Arnoldo Valle-Levinson · Mario A. Caceres · Oscar Pizarro

Received: 17 October 2012 / Accepted: 17 January 2014 / Published online: 12 February 2014

Abstract Residual, or tidally averaged, circulation in fjords is generally assumed to be density driven and two layered. This circulation consists of a thin surface layer of outflow and a thick bottom layer of sluggish inflow. However, development of different vertical structures in residual circulation in fjords can arise from wind, remote, and tidal forcing that may modify the two-layer circulation. Particularly, theoretical results of tidal residual flows in homogeneous semienclosed basins indicate that their vertical structure is determined by the dynamical depth of the system. This dynamical depth can be considered as the ratio between the water column depth and the depth of frictional influence in an oscillatory flow (inverse of Stokes number). When the frictional depth occupies the entire water column, the tidal residual flow is one layered as in shallow basins. But when the frictional depth is only a small portion of the water column (>6 times smaller), the tidal residual is three layered. In relatively deep fjords (say deeper than 100 m), where frictional depths typically occupy a small portion of the water column, the tidal residual flow is expected to be three layered. Ample observational evidence presented here shows a three-layered exchange flow structure in fjords. On the basis of observational and theoretical evidence, it is proposed that the water exchange structure in deep fjords (more than six frictional layers deep, or inverse Stokes number >6) is tidally driven and is three layered. The tidally driven three-layer structure of residual flows could be regarded in some cases as the fundamental structure. However, this structure will only be observed sporadically as it will be masked by wind forcing, remote forcing from the ocean, and freshwater pulses.

Keywords Fjord circulation · Three-layer flows · Tidal residual flow

Responsible Editor: Rockwell Geyer

This article is part of the Topical Collection on *Physics of Estuaries and Coastal Seas 2012*

A. Valle-Levinson (✉)
University of Florida, Gainesville, FL 32611, USA
e-mail: arnoldo@ufl.edu

M. A. Caceres
Facultad de Ciencias del Mar, Universidad de Valparaíso, Av. Borgoño, 16344 Viña del Mar, Chile

O. Pizarro
Universidad de Concepción, Barrio Universitario s/n, Concepción, Chile

1 Introduction

The typical tidally averaged or residual circulation in fjords is usually described as two layered and density driven (e.g., Geyer and Cannon 1982; Officer 1976). River discharge or glacier melting provides a source of freshwater that is thought to establish density gradients that drive the circulation. However, because of the greater depths of fjords relative to coastal plain estuaries, vertical mixing away from localized sills and coastline constrictions tends to be much weaker. Mixing in fjords occurs preferentially via wind stresses and internal wave breaking, in contrast to the influence of bottom stresses in shallow estuaries. Such difference in mixing allows the buoyant layer, derived from freshwater input, to occupy a small portion of the water column (<1/10) and to remain trapped above a sharp pycnocline throughout the length of the fjord. Horizontal density gradients within a fjord are therefore restricted to a small fraction of the water column, and yet, these gradients are routinely attributed as the main drivers of residual circulation (e.g., Officer 1976; Dyer 1997). At depths beyond those potentially influenced by density gradients, the residual flow in fjords is customarily taken as rather weak, i.e., close to zero. However, improved

technology in the observation of velocity profiles during the last two decades has illustrated a seemingly more complicated picture than previously explained. Three-layered residual flows in fjords can be ubiquitous and alter the typically described two-layer circulation. This three-layered circulation can arise mainly from the influence of wind forcing (e.g., Klinck et al. 1981), from density gradients outside the fjord (e.g., Stigebrandt 2012), or from tidal forcing (e.g., Valle-Levinson et al. 2007). The objectives of this study are (a) to document the presence of three-layered residual flows in fjords and (b) to provide a possible explanation for their development.

On the basis of theoretical studies (Ianniello 1977; Winant 2008), it is hypothesized that the residual circulation in "deep" fjords will be tidally driven and three layered. A thin (<10 m deep) surface outflowing layer is reinforced by buoyancy input and overrides an inflowing layer that occupies close to half the water column. Another outflowing layer develops beyond the inflowing mid-water layer. In this context, deep fjords are those where the depth is greater than six times the depth of frictional influence. The objectives and hypothesis are addressed by presenting existing theory and analysis of observations. Theoretical basis for the development of three-layer exchange flows, as driven by tides, is summarized in order to try to explain the relationship between expected and observed flow structures. Five observational examples (Fig. 1) of the development of three-layered residual exchange flows in different Chilean fjords provide support for the theoretical basis. In one of those five fjords, time series provide information on how persistent the three-layered flow structures can be. This study is more suggestive than conclusive but provides evidence to consider a three-layer tidal residual circulation in deep fjords.

1.1 Theoretical basis for development of three-layered residual flows

Theoretical results have been obtained by Ianniello (1977) and Winant (2008) for tidal residual flows in homogeneous, semienclosed rectangular basins connecting to an adjacent ocean. Ianniello (1977) solved a laterally averaged nonrotating momentum balance, including advective acceleration terms, over flat bathymetry in narrow channels that were weakly nonlinear. In weakly nonlinear channels, the ratio of

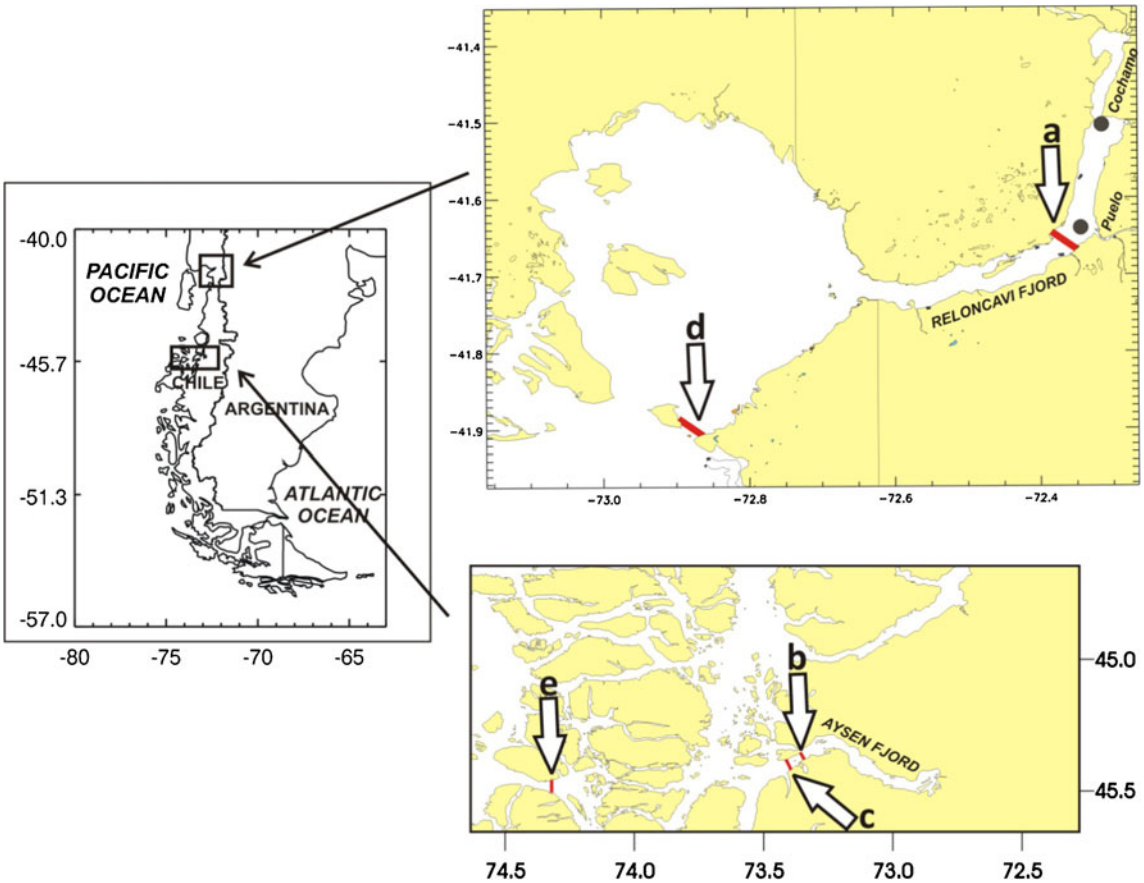

Fig. 1 Locations for observations illustrated in Figs. 2 and 4 through 9. Reloncavi fjord was the site of cross-fjord transect (**a**) and the deployment of two moorings (*black dots*). Aysen fjord was sampled for two cross-fjord transects (**b** and **c**). Paso Nao (**d**) and Canal Darwin (**e**) were sampled for one cross-fjord transect

tidal amplitude to total water depth is <<1, which is the case in deep fjords. Perturbation methods, valid in weakly nonlinear systems, were applied to obtain the tidal flow at the lowest order. Tidal flows were represented generically as damped waves subject to various eddy viscosity parameterizations. Solutions depicted typical tidal flow profiles that were not very sensitive to eddy viscosity formulations.

Tidal flows were in turn used by Ianniello (1977) to obtain the higher order flow: the tidally averaged or residual velocity profiles. These velocity profiles arose from a tidally averaged momentum balance among local plus advective accelerations, pressure gradient, and frictional influence. Solutions for tidal and residual flows provided profiles that depended mainly on a nondimensional number δ that compared local accelerations of along-basin flow ($\partial u/\partial t$) to frictional effects. Frictional influence was expressed as the vertical contribution from the stress divergence ($\partial \tau /\partial z$, where τ is the shear stress given by the product of the vertical eddy viscosity A_z and the vertical shear of horizontal currents $\partial u/\partial z$). Scaling $\partial u/\partial t$ as $U\omega$ (where ω is the frequency of tidal forcing) and $\partial\ [A_z\ \partial u/\partial z]/\partial z$, the stress divergence, as $A_z\ U/H^2$ (where H is the maximum depth), the ratio δ can be written as:

$$\delta = \sqrt{\frac{\omega H^2}{A_z}} \tag{1}$$

Equation 1 is the inverse of the Stokes number (e.g., Huijts et al. 2009) and can also be regarded as the ratio of the water column depth H to the depth of frictional influence caused by an oscillatory flow $A_z/(\omega H)$. The latter is analogous to the Ekman depth of frictional influence, as it indeed becomes the Ekman depth if the frequency of the oscillatory motion is replaced by the inertial frequency (or Coriolis parameter).

Ianniello's (1977) theoretical Eulerian residual flows depended on δ. For δ values of 1 or 2, the residual Eulerian flow was seaward throughout the water column, and for δ between 3 and 5, the residual flow was two layered with inflow at the surface and outflow underneath. For basins where $3<\delta<5$, the tidal residual flow competes with the gravitational circulation. A crucial result was a three-layered Eulerian flow that developed when $\delta\geq 6$ (water column depth six or more times greater than frictional depth). This three-layer structure consisted of outflow at the surface and bottom, with inflow in the middle (red and blue lines in Fig. 2a). There are three main mechanisms that produce this type of tidally driven residual exchange flow. The mechanisms were not addressed explicitly by Ianniello (1977) but were explained by Li and O'Donnell (2005). One is the Stokes transport into the basin caused by the tidal wave. Another drives residual outflow from the response to the residual water level setup, caused by the Stokes transport. The third mechanism is related to spatial gradients in tidal flow, or tidal stresses. These three mechanisms compete to shape the residual flow. For standing or near-standing waves, as in many fjords, the tidal stresses become the main driving mechanism of tidal residual flows.

Parallel to Ianniello's (1977) work, Winant (2008) has generated analytical solutions in systems with lateral variations in bathymetry. In this way, Winant relaxed the restriction of lateral uniformity in bathymetry and flow, plus allowed solutions for lateral flows. In addition, Winant's solution considered the effects of the earth's rotation. The spatial structure, laterally and with depth, of Winant's (2008) tidal residual flows also depended on the ratio δ. Moreover, the lateral structure depended on the ratio κ between the basin's length L (multiplied by 2π) and the tidal wavelength, or $(gH)^{0.5}/\omega$, where g is gravity's acceleration. Both δ and κ were influenced by H and ω in such a way that knowledge of the basin's length L and the value of δ allowed inference of the value of κ. This is because prescription of δ implied knowledge of A_z. The main point is that δ was a key parameter to Winant's solution, in the same way that it was for Ianniello's. Consistently, Winants's (2008) tidal residual flows in both Eulerian and Lagrangian reference frames for a basin with δ of 10 were three layered (Fig. 2b). Residual outflow was found at the surface and bottom layers, and residual inflow developed in an intermediate layer. Some lateral variability in exchange flows was related to bathymetric variations across the basin. Nonetheless, both Ianniello's and Winant's theoretical results indicated that tidal residual flows in relatively deep basins (where $\delta>6$) were expected to show outflow at the surface and bottom, separated by an inflowing layer. Theoretical results were consistent with five observational examples shown in Fig. 3 and described next.

1.2 Observations of spatial structure of residual circulation

Observations of the transverse and vertical structure of mean flow after one tidal cycle in the middle of Reloncavi fjord (Fig. 1) showed a three-layered structure (Valle-Levinson et al. 2007). According to Eq. 1, the depth of frictional influence δ at the section of measurements is between 30 and 100. These values of δ are obtained using A_z between 1×10^{-3} and 1×10^{-4} m^2/s, H of 100 m and ω of 0.00014 s^{-1}. Residual outflow in Reloncavi fjord appeared in two layers: a thin surface layer (<10 m) and a layer below the depth of ~80 m (Fig. 3a). A ~70-m thick layer of inflow appeared between the two outflowing layers. This apparently puzzling three-layer structure was also observed in the mean flow profiles of ~1.5-month deployments of current profilers at the mouth and in the middle of the same Reloncavi fjord (Castillo et al. 2012). However, this has not been the only Chilean fjord or inlet where the observed mean circulation consisted of three layers. Three other systems are illustrated here through four more examples, as two cases come from the

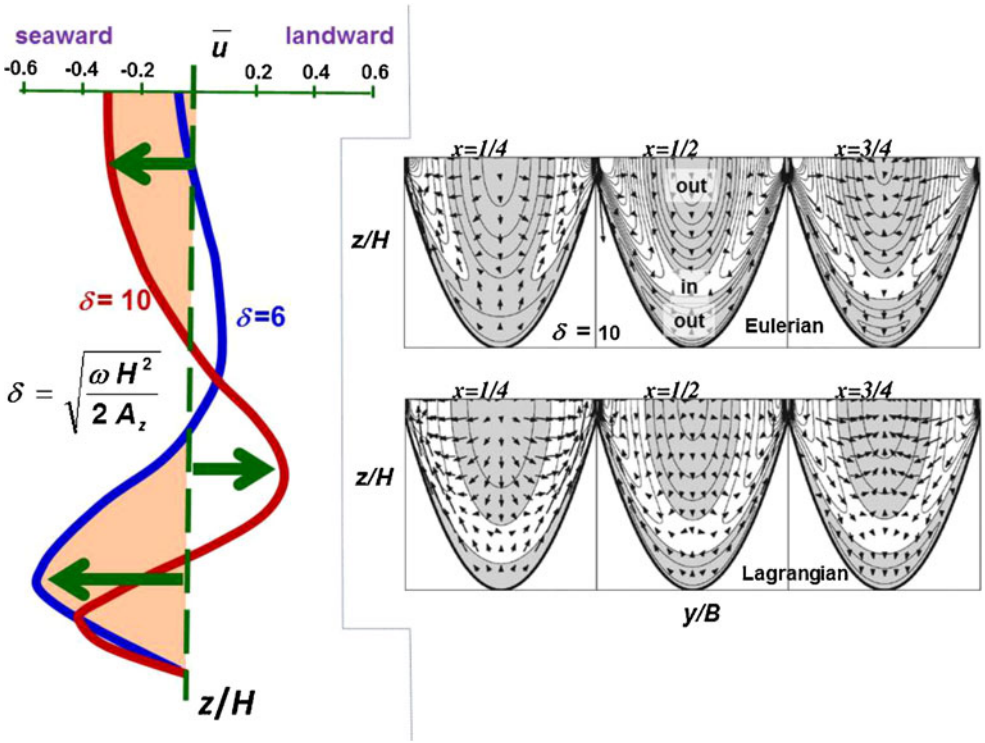

Fig. 2 Theoretical results for tidal residual flows in deep basins. The *left part* of the figure reconstructs Ianniello's (1977) results for water columns in which there are six and 10 frictional layers (δ equals six and 10). Both cases portray a three-layer residual flow. The *right part* of the figure displays the theoretical results of Winant (2008) for Eulerian and Lagrangian tidal residuals at different cross-sections along a semienclosed basin where δ equals 10. The sections are located at nondimensional distances of x=¼, ½, and ¾ from the basin's head. Views are landward with nondimensional distance across the basin y of width B and nondimensional depth z/H. *Gray-shaded contours* represent residual outflow (toward observer) and *arrows* denote lateral flows that are not discussed here

same fjord. Several other fjords with depths >150 m have exhibited qualitatively the same flow structure (Cáceres, unpublished data).

In all examples in Fig. 3, data were collected at a cross-channel transect with a 307.2-kHz Teledyne Instruments acoustic Doppler current profiler (ADCP) that was mounted on a catamaran and towed for at least one tidal cycle. A Global Positioning System (GPS) was used for navigation to record position data and to correct the ADCP compass following Trump and Marmorino (1997) and Joyce (1989). Vertical resolution of current velocity profiles was 2 to 4 m, with maximum profiling range of 150 m for reliable current velocity values. Sampling transects were repeated more than 10 times and were transformed from the original irregularly spaced to regularly spaced velocity data (e.g., Valle-Levinson and Atkinson 1999). Time series at each grid point of the regularly spaced data were separated into tidal and residual flow contributions to the observations (e.g., Valle-Levinson and Atkinson 1999). Only residual or tidally averaged flows are shown and represent conditions during different times of the year. Residual outflow appears consistently near the surface and near the bottom, while inflow develops between the outflowing layers. The layer of surface outflow was rather shallow and nearly undetectable in Aysen Fjord on October 16, 1998 (Fig. 3b) because of the coarse vertical bin size (4 m), which gave the first measurement at 8 m (Cáceres et al. 2002). At another transect of the same Aysen Fjord measured on November 17–18, 2001 (Fig. 3c), the near-surface resolution was the same as on October 16, 1998 and the exchange flow was remarkably similar (Cáceres et al. 2010a). The commonality of the three examples described thus far is that the water column displayed a shallow pycnocline, distributed throughout the first 10 m of the water column.

The other two examples in Fig. 3 that illustrate the three-layer exchange flow showed a well-defined surface layer and weaker stratification than in the other examples. Residual flows in Nao Pass (Fig. 3d) were obtained on November 13–14, 2004 (Cáceres et al. 2010) and showed lateral variations, in addition to the vertical segregation in three layers as in the transects of the other sites. Those lateral variations were attributed to marked changes in bathymetry (Valle-Levinson 2008). Finally, residual flows at Darwin Channel in the archipelago between the Pacific Ocean and the Inland Sea (Fig. 3e) showed the example with the best defined three-layer structure (Castillo et al. 2006). It is clear, then, that the three-layered residual flow structure is not an oddity in the entire region of the Chilean Inland Sea. A question that arises is whether this structure is density driven, tidally driven, or wind driven. The possible influence of density gradients and wind stress on the three-layer flow structure is addressed in the "Discussion." It is proposed here that the most likely cause for the three-layer flow structure is tidal forcing, as suggested by theoretical results of tidal residual flows in semienclosed basins. To generate three-layer residual flows, the basin's depth should be several times greater than the depth of frictional influence,

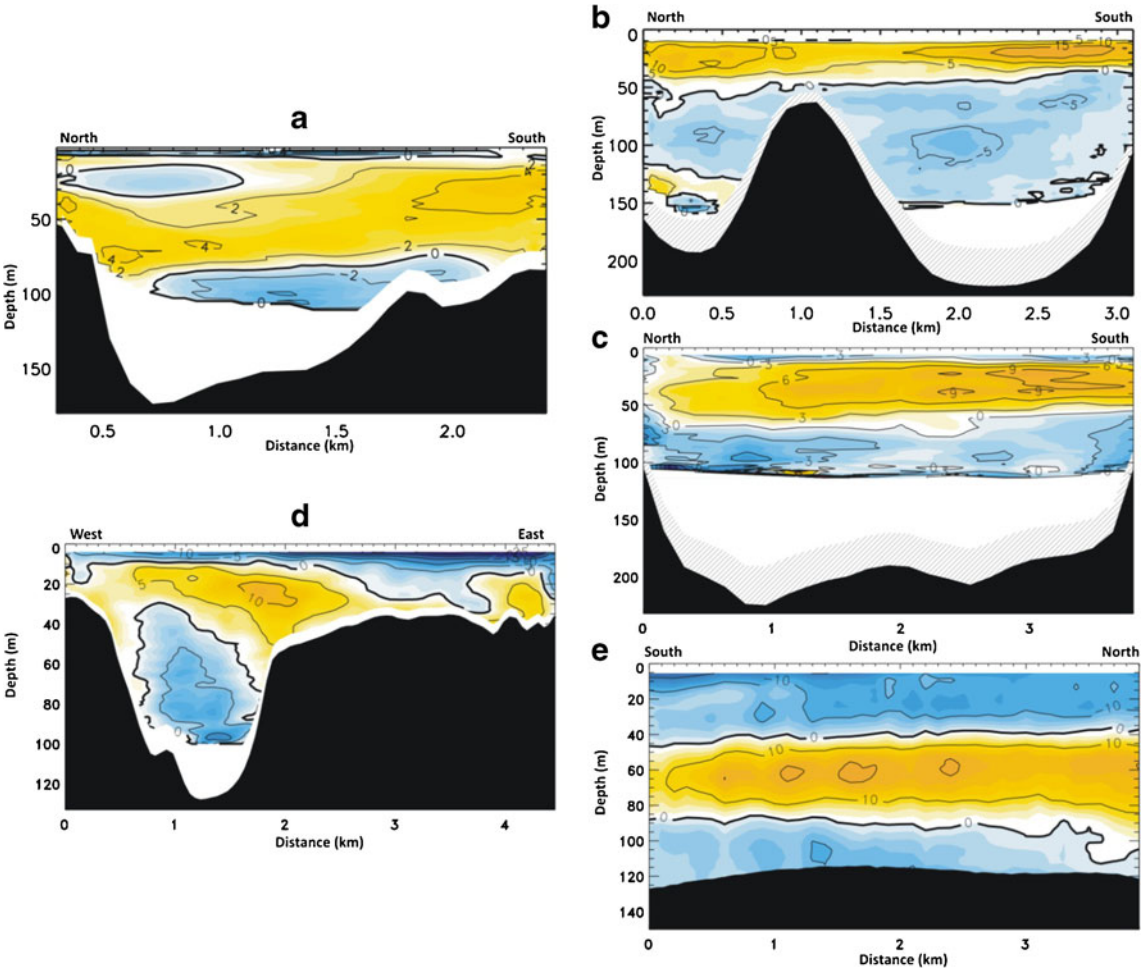

Fig. 3 Residual flows (in centimeters per second) obtained throughout complete tidal cycles at the fjords portrayed in Fig. 1. **a** Reloncavi fjord. **b** and **c** Aysen fjord. **d** Paso Nao. **e** Canal Darwin. All figures, except Canal Darwin, are looking landward and illustrate three-layered residual exchange flow. Locations in Fig. 1 with the same letters. *Blue regions* denote residual outflows, while *orange regions* indicate inflows

as explained in the previous section. All cross-sections displayed in Fig. 3 were characterized by δ values of at least 10.

One could argue that the persistence of the three-layered flow structure observed in Fig. 3 was fortuitous, even though sampling was indiscriminate with respect to locations and time. However, all these and other unreported three-layered flow structures in the area have been collected under weak wind conditions, which actually allowed shipboard operations. A total of 49 experiments of towed ADCPs have been carried out in different locations of the northern Patagonia Chilean fjords from 1998 to date (the authors of this study have been directly or indirectly involved in all 49). The sites of these experiments roughly cover most of the main channels and fjords of the region. Results have shown three-layer exchange flows in 17 (35 % of total) tidal-cycle or 24-h experiments, all of them in transects >100 m deep. Other transects showed either the typical two-layer gravitational circulation (in systems with freshwater influence and tidal currents ~1 m/s) or laterally sheared exchange flows (in systems with no freshwater influence and tidal currents >1 m/s). Generalities in exchange flow structures can begin to be drawn on the basis of tidal forcing and buoyancy (river) input. Therefore, the three-layer flow structure appears to be persistent in deep fjords when atmospheric and remote forcing are insubstantial. The next issue to investigate is whether the three-layer flow structure can be observed persistently in time series of velocity profiles that are longer than 1 day. In order to address this issue, two time series obtained in Reloncavi fjord were analyzed.

1.3 Temporal variability of residual velocity profiles

Two upward-pointing acoustic Doppler current profilers (ADCPs) were deployed near the head and in the middle of Reloncavi fjord. Data from these instruments were used to determine the temporal variability of residual velocity (or the variability of tidally averaged flow, i.e., the low-pass-filtered flow) profiles in a fjord where three flow layers had been observed (Fig. 3a). A 614.4-kHz ADCP was moored at Cochamo (41°29.794′S, 72°19.176′W), near the coastline

constriction toward the head of the fjord over a water column depth of 114 m. The instrument itself was deployed on a taut-wire at a mean depth of ~61 m from July 13, 2006 to February 17, 2007. Data were recorded every 15 minutes in 2-m bins, representing ensemble averages of 85 1-s pings and giving a measurement standard deviation of 0.3 cm/s. Remarkably, the acoustic intensity data indicated that there were not enough scatterers near the surface (shallower than 40-m depth) during daylight hours to provide measurements of velocity from July 13 until August 30, 2006. Most likely, the lack of scatterers was related to the absence of planktonic populations near the surface during light hours because of diel vertical migrations (e.g., Rippeth and Simpson 1998). But the topic of diel migrations requires full attention in a separate study because of their peculiarities at the sampling site. In relevance to this study, diel migrations caused velocity measurements to be biased in favor of flood from July 13 to August 30, 2006, and therefore, only the record after that date is analyzed. This record location will be referred to as *up-fjord* site.

The second ADCP was moored in the middle of the fjord, where it changes orientation, off the region of the Puelo River discharge (41°37.830′S, 72°20.802′W). The ADCP operated with a frequency of 307.7 kHz pointing upward at a depth of 122 m over a water column of 177 m. Data were recorded every 15 minutes also from July 13, 2006 to December 16, 2006 in 5-m bins with 40 1-s bursts, yielding a measurement standard deviation of 0.4 cm/s. The absence of near-surface acoustic backscatterers during daylight also affected the record from the start of the deployment until September 5. Therefore, the initial portion of the record was excluded from analysis. This location will be referred to as *mid-fjord* site.

Water velocity data profiles were first rotated to the axis of maximum variance in such a way that the up-fjord and mid-fjord sites were aligned −5° and 1° from magnetic North, respectively. Subtracting the magnetic declination of 8.5° at that location and time yields rotations of −13.5°T and −7.5°T (degrees from true north), respectively. Profiles of the subtidal along-fjord flow component were then obtained using a Lanczos filter with a half-power of 40 h to eliminate tidal and inertial effects on the flows. Finally, an analysis of Empirical Orthogonal Functions (EOFs) was carried out separately on the two low-pass-filtered time series of along-fjord velocity profiles at the up-fjord and mid-fjord locations. The essence of an EOF analysis is to construct the covariance matrix of all the velocity time series, related to velocity profiles, at one site and solve the eigenvalue problem related to the covariance matrix. Solution to this problem yields the spatial structure of the time series (the eigenvectors) and the temporal variability of the eigenvectors (the principal components). The eigenvectors represent dominant vertical structures of the horizontal velocity. Thus, a three-layered structure in the eigenvectors represents the three-layered flow that is sought in the descriptions during the instances in which the principal components display the largest amplitudes.

An advantage of using EOF analysis over a mere description of the low-pass-filtered flow profiles is that the latter, the flow profiles, do not show a clear and consistent structure throughout the deployment. At first glance, the low-pass-filtered velocity profiles at the up-fjord site (Fig. 4) revealed values of up to 0.15 m/s and variations with periods of a few days. Also, there seemed to be more outflow (blue contours) near the surface and more inflow (yellows and reds) toward depth. This suggests that, on average, there was residual outflow at the surface and residual inflow at depth, i.e., gravitational circulation. In fact, the temporal mean of all the profiles (lower panel of Fig. 4) indicated the influence of gravitational circulation with ~0.05 m/s residual outflow and 0.02 m/s inflow. Most of the mean outflow was concentrated in the ~10 m surface pycnocline layer, although some more outflow appeared down to ~20 m from the surface. Moreover, looking again at the subtidal variations in velocity profiles, it was evident that there were sporadic periods in the record that exhibited negative (blue) contours near the bottom. Negative flows indicated residual outflow and, at times, a three-layered exchange flow (e.g., days 250, 330, 370). However, no clear relationship could be gleaned from this representation between fortnightly tidal forcing (upper panel in the figure) and residual (low-pass-filtered) flows. If the three-layer flows are related to tidal forcing, some relationship should be expected between spring tides and residual flows.

At the up-fjord location, the first three orthogonal modes explained 91 % of the variability observed, with 60 % related to mode 1, 23 % to mode 2, and 8 % to mode 3. The eigenvectors derived from the orthogonal functions described the subtidal velocity profiles associated with each mode. Mode 1 eigenvectors (Fig. 5) depicted two-layer flows while modes 2 and 3 described three-layer structures. The three-layer profiles are compatible with residual circulation associated to tidal forcing in deep systems (δ>6). As seen, modes 2 and 3, combined, explained 31 % of the variability in such a way that three-layered residual circulation at this fjord's site was not uncommon.

The temporal variation of the orthogonal modes, or principal components (Fig. 5), describes when each mode was influential on the observed signal. Inspection of the principal components indicated variability with dominance of a few days but no distinct period. However, a 7-day low-pass-filtered version of the principal components revealed a clear modulation related to fortnightly variability. This was a first indication that modes 2 and 3 had influence from the tides through fortnightly modulation. Spectral analyses of the principal components confirmed the periods that dominated their variability (Fig. 6). The energy spectrum of mode 1 showed peaks at periods of 4 and 5 days connected to the passage of weather systems that affected the fjord region. Mode 2 was

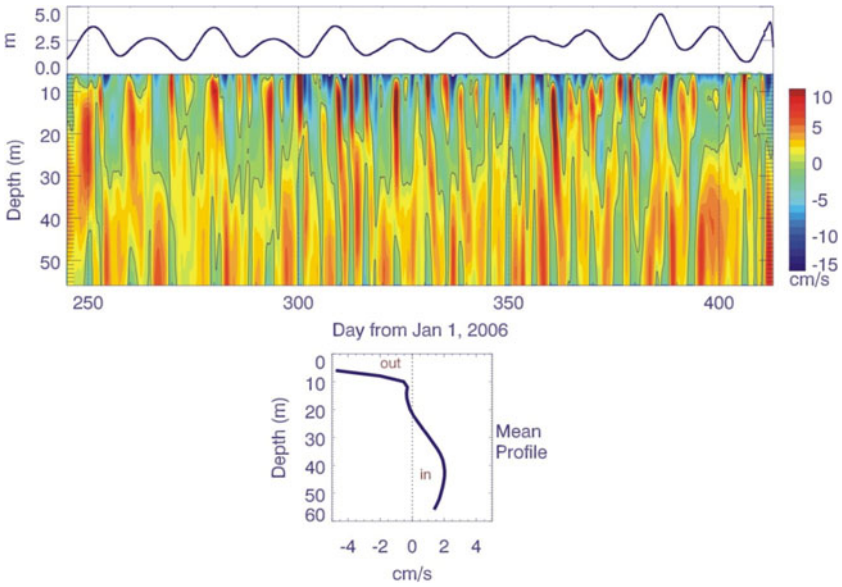

Fig. 4 Observations of tidal amplitude (*upper panel*), low-pass-filtered along-fjord flow profiles (*middle panel*), and deployment-long along-fjord mean flow profile (*lower panel*) at the up-fjord location, i.e., at Cochamo (total depth of 114 m). In the *middle panel*, negative values (in *blue*) denote residual outflow and the *vertical axis* represents depth. Also in the *middle panel*, the *line contour* indicates 0 m/s, the interface between residual outflow and inflow

dominated by fluctuations of 14.3 days related to fortnightly tides and of 5 days associated with atmospheric forcing. Mode 3 was influenced mostly by oscillations with dominant periods of 14.3 days, i.e., by tidal fortnightly variability. Spectral distributions, then, indicated that gravitational two-layer circulation was modified by atmospheric forcing, while the three-layer circulation was mostly modulated by spring-neap tides but also by atmospheric forcing as in mode 2.

A coherence analysis (correlation at different frequencies) between water level and each mode 2 and 3 at the up-fjord location confirmed the fortnightly character of the fluctuations (Fig. 7). At the up-fjord site (left panels of Fig. 7), there were statistically significant correlations (coherence squared values above the horizontal dashed line) between water level and mode 2 and also mode 3 at fortnightly frequencies (vertical dotted blue line). Mode 2 showed the highest correlations at periods close to 24 days, near tidal monthly variations, while mode 3 was dominated by fortnightly correlations. The phase values derived from the coherence analysis indicated a ~−110° lag between subtidal forcing and mode 2 and a ~−60° lag with

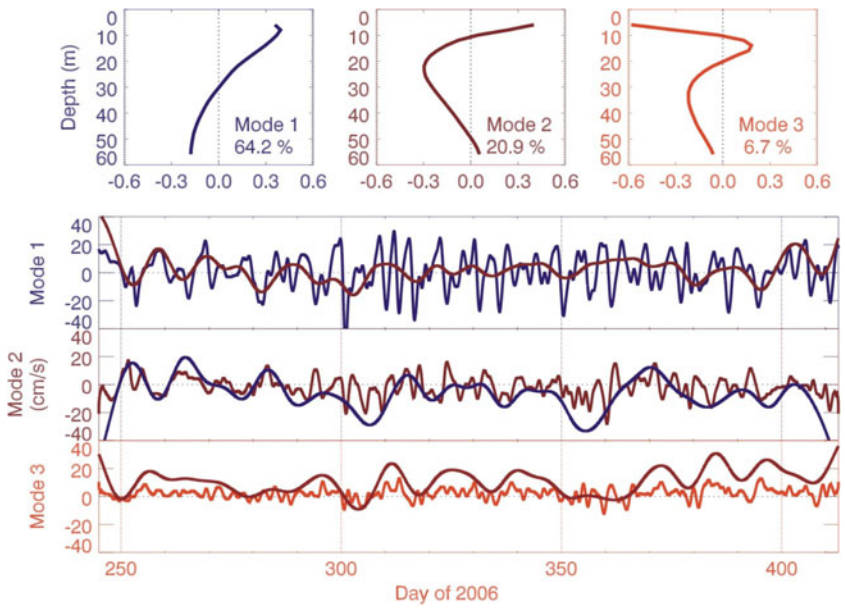

Fig. 5 Up-fjord location eigenvectors and principal components (or temporal evolution of eigenvectors) for the three empirical orthogonal functions that explain most variability of the flow portrayed in the middle panel of Fig. 4. The *upper row* of figures illustrates the eigenvectors, or spatial structure of the flow with depth for each mode. Underneath the eigenvector profiles, the temporal variations of the principal components are shown together with their 7-day low-pass-filtered versions, which were multiplied times factors of 3, 4, and 5, respectively, to facilitate visualization of their fluctuations. The product of eigenvectors and principal components yields units of centimeters per second

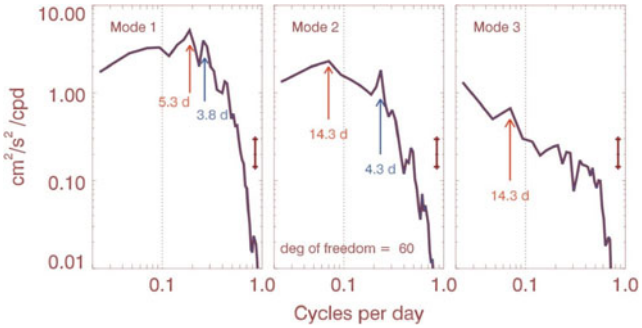

Fig. 6 Spectral energy of the three main principal components at the up-fjord location. *Arrows* indicate the most energetic peaks and their period

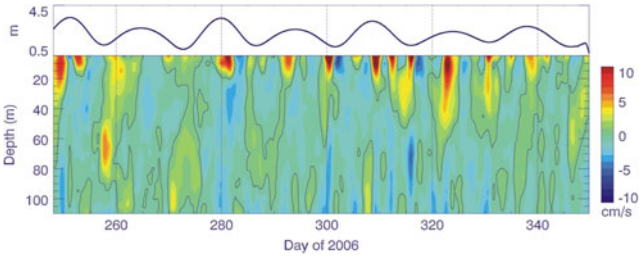

Fig. 8 Observations of tidal amplitude (*upper panel*) and low-pass-filtered along-fjord flow profiles (*lower panel*) at the mid-fjord location, i.e., at Puelo (total depth of 177 m). In the *lower panel*, negative values (in *blue*) denote residual outflow and the *vertical axis* represents depth. Also in the *lower panel*, the *line contour* indicates 0 m/s, the interface between residual outflow and inflow

mode 3. These phase lags represented the eigenvector profiles for modes 2 and 3 with inverted signs, and with a temporal phase lag between the highest tidal range and the strongest three-layered flows. Thus, the analysis gave further evidence, albeit tenuous, of the tidal origin of the three-layered residual flows.

At the mid-fjord location, subtidal flows were also highly variable with no discernible structure in time or with depth (Fig. 8). Gravitational flow was evident with outflow (blue) at the surface and inflow (yellow or red) underneath during some periods. However, inflow at the surface and outflow underneath developed during other periods. Further inspection of subtidal flows (Fig. 8) suggests that synoptic-scale fluctuations dominated the signal. Once again, the variability was not obviously related to fortnightly tidal modulations so the EOF analysis was used to elucidate the main features of the record, both in depth and in time. The first three EOF modes, together, explained 87 % of the variability, with 56 % attributed to mode 1, 21 % to mode 2, and 10 % to mode 3. Eigenvectors of mode 1, representing the dominant vertical structure of the observed subtidal currents, displayed two layers (Fig. 9), as discerned in the description of Fig. 8. Similarly to the up-fjord location, modes 2 and 3 exhibited a three-layered structure at this mid-fjord site. Coincidentally, both modes, together, explained 31 % of the flow variability as was the case for the up-fjord measurements.

Similar to the principal components of the up-fjord location (Fig. 5), the principal components of the mid-fjord location were dominated by synoptic-scale and fortnightly fluctuations (Fig. 9). A 7-day low-pass filter applied to all three principal components showed fortnightly fluctuations dominating modes 2 and 3, but not as evident in mode 1. Mode 1 had its largest fluctuations at periods shorter than the fortnightly, most likely related to synoptic-scale forcing. This was again confirmed with spectral analysis of the principal component time series. Spectral energy of the principal component of mode 1 indicated dominant variability at periods of 3.5 and 7.5 days

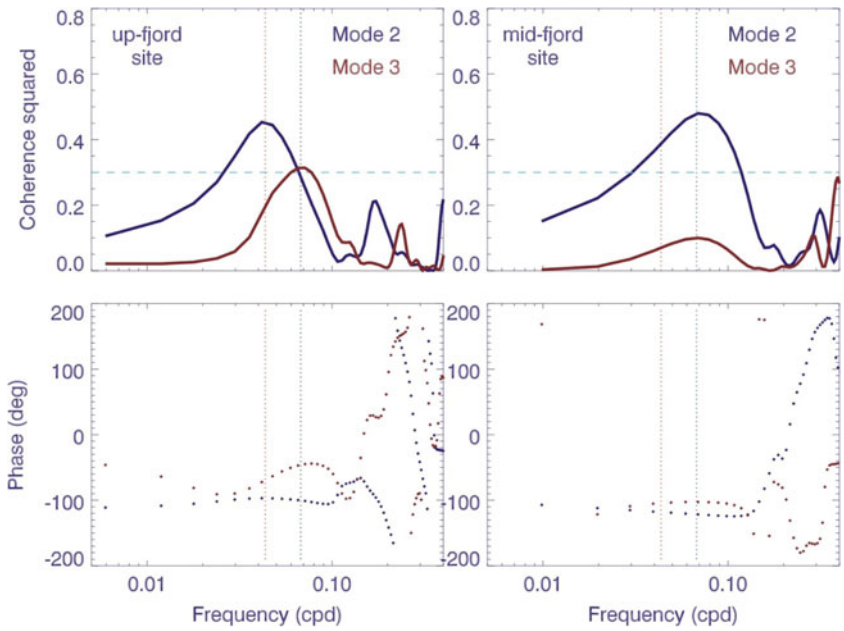

Fig. 7 Coherence squared and phase between water level and EOF mode 2 (*blue*) and 3 (*red*) for the up-fjord site (*left panels*) and mid-fjord site (*right panels*). The horizontal *dashed line* at a coherence squared value of ~0.3 represents the 90 % significance level. *Vertical dotted lines* indicate frequencies associated with fortnightly (*blue*) and ~24 day (*red*) variations

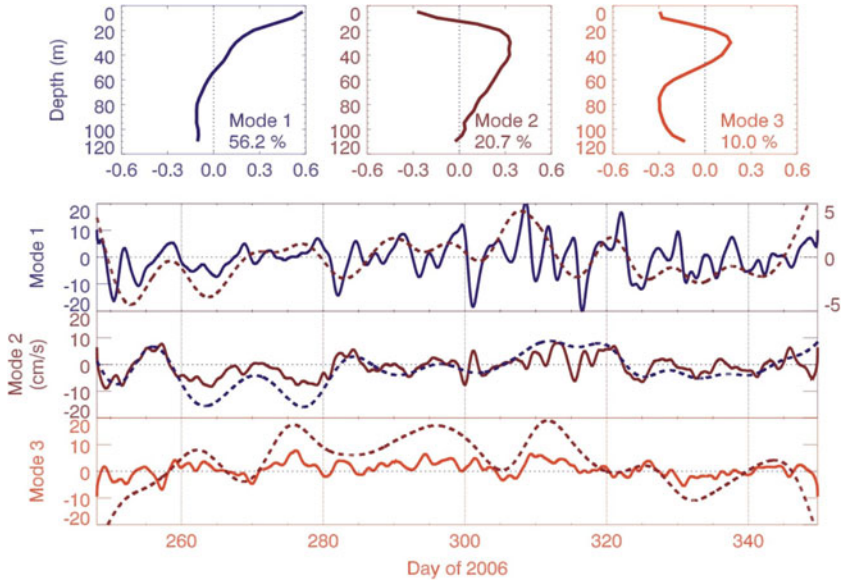

Fig. 9 Mid-fjord location eigenvectors and principal components (or temporal evolution of eigenvectors) for the three empirical orthogonal functions that explain most variability of the flow portrayed in the *lower panel* of Fig. 8. The *upper row* of figures illustrates the eigenvectors, or spatial structure of the flow with depth for each mode. Underneath the eigenvector profiles, the temporal variations of the principal components are shown together with their 7-day low-pass-filtered version, which were multiplied times factors of 1, 3, and 5, respectively, to facilitate visualization of their fluctuations. Note the different *axis* on the right for the 7-day low-pass-filtered version of mode 1. The product of eigenvectors and principal components yields units of centimeters per second

(Fig. 10). The spectral energy of mode 2 was dominated by periods of 14.3 and 8 days related to tidal fortnightly and atmospheric forcing scales, respectively. Finally, mode 3 showed spectral energy governed by periods of 14.3 days (Fig. 10). Both the up-fjord and mid-fjord stations showed three-layered subtidal flows influenced by fortnightly variations. At the mid-fjord location, there was a significant correlation between water level and mode 2 at fortnightly frequencies (Fig. 7 right panels). Mode 3 showed also a peak at fortnightly frequencies although the correlation was not statistically significant (Fig. 7). The apparent tidal modulation of the three-layered flow structure suggested that tides were the main drivers of such circulation, as also proposed by the theoretical solutions of Ianniello (1977) and Winant (2008).

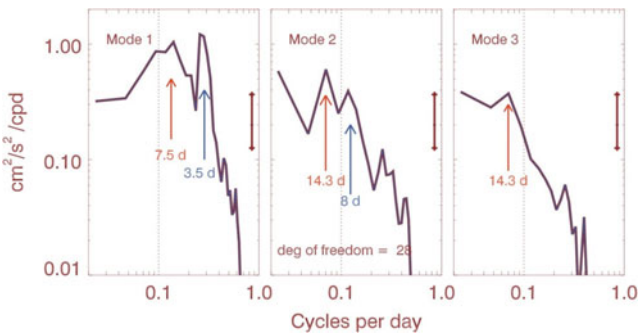

Fig. 10 Spectral energy of the three main principal components at the mid-fjord location. *Arrows* indicate the most energetic peaks and their period

2 Discussion

There are two aspects that require more discussion with respect to the three-layer circulation in fjords as observed in the towed ADCPs (Fig. 3) and in the moored ADCPs in Reloncavi fjord (Figs. 5 and 9). One has to do with the possibility of the three-layer circulation in fjords being driven by wind or by density gradient, instead of by tides. The other aspect has to do with the fact that the moored observations presented here occupied only 0.5 of the water column at the up-fjord location and 0.6 of the water column at the mid-fjord location, leaving an important part of the water column unresolved.

First, is the three-layer flow driven by wind, density gradients, or tides? Other studies in fjords have shown that wind-driven circulation outside the fjord can influence the subtidal circulation in the fjord (e.g., Klinck et al. 1981; Svendsen and Thompson 1978; Stucchi and Bell 1980). Wind-driven coastal currents can reverse the gravitational circulation and change the residual transport inside the fjord. Even though there were no wind data available for the period of observations with the moored ADCPs, it is most likely that the flow reversals observed near the surface (red-filled contours in Figs. 4 and 8) were related to this situation. On the other hand, those previous studies also indicated that along-fjord winds cause a local response, changing the sea-surface slope and isopycnal tilt inside the fjord, but produce little variations in volume transport. Winds that are directed up-fjord tend to oppose the gravitational circulation and can drive three-layer flows (e.g.,

Klinck et al. 1981). This was likely the case documented by EOF mode 2 that exhibited some synoptic-scale variability. However, all cases of three-layer exchange flow observed during cross-fjord surveys, as documented in Fig. 3, were not influenced by wind. When wind is influential in the study area, shipboard data quality is greatly hampered or conditions hinder any data collection. Therefore, wind was not the sole agent that caused the three-layer flow structure in these measurements.

Similarly to three-layer flows driven by wind, there have been studies that have suggested that density gradients can produce three-layer flows in <20-m deep waters (e.g., Chao et al. 1996) and in >40-m deep waters (e.g., Valle-Levinson et al. 2001; Stigebrandt 2012). There are several ways in which density-driven three-layer flows can develop in semienclosed basins. One way occurs when the basin has relatively homogeneous density near its head, and this density is intermediate to the stratified density in the waters adjacent to the basin. In this situation, residual flows advance toward the head of the basin at the surface and bottom and out of the basin in an intermediate layer (Chao et al. 1996). A second way for density-driven three-layer flows to appear is through enhanced mixing over a shoal or sill in a stratified basin. Such enhanced mixing will cause intermediate density relative to an upper buoyant layer and a lower dense layer, adjacent to the shoal or sill. The horizontal density gradients thus generated will cause, on the landward side of the sill, outflow at the surface and bottom and inflow over an intermediate layer (e.g., Valle-Levinson et al. 2001; Caceres, unpublished data at Meninea Strait). Even a third way is through density variations outside a fjord. In this case, however, the density outside the fjord becomes intermediate between the buoyant and deep layers inside the fjord and both the intermediate and deep layers flow into the fjord (e.g., Stigebrandt 2012; Straneo et al. 2010). Occasionally, deep layers can flow out of a silled fjord when deep densities outside are lower than those inside the fjord (e.g., Arneborg 2004).

Clearly, none of the three viable scenarios was possible in Reloncavi fjord, site of the moored records and the example of Fig. 3a. This was because of (a) the lack of sill or locally homogeneous waters that could affect the entire basin in the first two scenarios (Castillo et al. 2012), and (b) the near-bottom layer flowed seaward for the third scenario. The same (lack of a sill) can be said about the transects at Nao Pass and Darwin Pass (Figs. 3d, e). At Aysen Fjord, there is a sill-like feature, more like a seamount, portrayed in Fig. 3b. But hydrographic data at this part of the fjord indicated no evidence for mixing between the buoyant layer and oceanic waters. In this fjord, the pycnocline is restricted to intratidal vertical excursions of order 1 m with negligible tidal variations of salinity within the buoyant layer. There seems to be enough evidence to discard the scenario of density gradients as potential drivers of the three-layer exchange flows exemplified here. But additional targeted investigations are required to confirm such neglect of density gradients.

The results presented in this study allow the proposition that the natural state of relatively deep fjords is to exhibit a tidally driven three-layer residual flow. In this context, deep fjords are those where the depth is more than six times greater than the depth of frictional influence. In such deep systems, the input of freshwater should represent a thin (<10 % the water column depth) layer of buoyant fluid that forces its way seaward and that ultimately could reinforce the tidally driven surface outflow. In the survey data of Figure 3, the best developed three-layer exchange flows developed at Nao Pass and Darwin Pass, where there was no clear pycnocline. Generally, in deep fjords with no wind, density gradients, or remote forcing, the residual flow should then be tidally driven and three layered. This three-layered state, however, could be reinforced or obscured by wind forcing, which is ubiquitous and energetic (typically ~0.1 Pa) in fjord regions. Three-layer flows could also be masked by pulses of freshwater discharge, related to frequent storms, which would cause deepening and shoaling of the pycnocline. Finally, it could be altered by remote forcing driving unidirectional flows throughout the water column by means of pressure gradients superimposed on those inside the fjord (e.g., Stigebrandt 2012; Arneborg 2004). In addition to the Chilean examples presented here, it could be argued that the winter circulation in Juan de Fuca Strait is consistent with the concepts proposed (Figs. 6 and 10 of Thomson et al. 2007). Although, in that case, the remote influence from upwelling is evident. Numerical experiments are already being carried out and should be further pursued in the future to challenge these suggestions, which are anchored in analytical solutions (Ianniello 1977; Winant 2008) and observations (Fig. 3).

As a final point of discussion, it should be mentioned that the mooring coverage for the two sites explored in this study was half of the water column at the up-fjord location and nearly two thirds at the mid-fjord location. Obviously, this coverage did not allow definitive resolution of the three layer-flows at either of the mooring sites. This is why deployment-long averages may show two layered, instead of three-layered flows. Nonetheless, these data provided reasonable evidence for three-layer flows in EOF modes 2 and 3 at both sampling sites. Remarkably, the separate EOF analysis at both sites yielded approximately the same variability of the records explained by the combination of modes 2 and 3 (~31 %). Future studies will concentrate in carefully trying to resolve the entire water column. In fact, a study by Castillo et al. (2012) resolved the entire water column near the mouth of Reloncavi fjord. The mean flow they obtained over ~40 days of deployment exhibited the three layers portrayed here. A 40-day mean should cancel out variations produced by wind forcing and variations in density gradients (e.g., Wong and Valle-Levinson 2002).

3 Conclusions

Observational evidence allows proposing an additional scenario of residual circulation in fjords, supported by theoretical arguments. In particular for deep fjords, the residual circulation is suggested to be three layered and tidally driven. Deep fjords are those where the water column depth is six or more times greater than a depth of frictional influence (as also represented by the inverse of the Stokes number). The three-layered circulation structure is expected to be masked by winds, which are frequent and energetic in fjord regions, by remote forcing and by rapid changes in river discharge. Further observational and new numerical studies will have to be undertaken to test the proposed scenario even further.

Acknowledgments Current data from moorings deployed in 2006 at Reloncavi Fjord were obtained under project CONA-C12F 06–02 supported by National Oceanographic Committee of Chile. A.VL acknowledges support from NSF project 0825876 and a Fellowship under Program of Short Stays 801100008 supported by CONICYT (Chile), to analyze some of the data at Universidad de Valparaiso. A.VL also acknowledges support from the Fulbright Commission and CSIC, Spain, which allowed completion of this document. Comments from two anonymous reviewers helped clarify several aspects of this presentation.

References

Arneborg L (2004) Turnover times for the water above sill level in Gullmar Fjord. Cont Shelf Res 24:443–460

Cáceres M, Valle-Levinson A, Sepulveda H, Holderied K (2002) Transverse variability of flow and density in a Chilean fjord. Cont Shelf Res 22:1683–1698

Cáceres M, Valle-Levinson A, Fierro J, Valenzuela C, Castillo M (2010a) Variabilidad transversal del flujo y de la densidad en la boca del Fiordo Aysén. Ciencia y Tecnología del Mar 33(1):5–15

Cáceres M, Valle-Levinson A, Belmar J, Bello M, Castillo M (2010b) Variabilidad transversal del flujo y salinidad en Paso Nao. Ciencia y Tecnología del Mar 33(2):45–58

Castillo M, Bello M, Reyes H, Guerrero Y (2006) Patrones de corrientes y distribución vertical de temperatura y salinidad en la entrada oceánica del Canal Darwin en invierno y primavera de 2002. Ciencia y Tecnología del Mar 29(2):5–21

Castillo M, Pizarro O, Cifuentes U, Ramirez N, Djurfeldt L (2012) Subtidal dynamics in a deep fjord of southern Chile. Cont Shelf Res 49:73–89

Chao S-Y, Boicourt WC, Wang HVC (1996) Three-layered circulation in reverse estuaries. Cont Shelf Res 16(10):1379–1397

Dyer, K. R. (1997), Estuaries, a physical introduction 2nd Edition, Wiley, 195 pp.

Geyer WR, Cannon G (1982) Sill processes related to deep water renewal in a fjord. J Geophys Res 87:7985–7996

Huijts KMH, Schuttelaars HM, de Swart HE, Friedrichs CT (2009) Analytical study of the transverse distribution of along-channel and transverse residual flows in tidal estuaries. Cont Shelf Res 29: 89–100. doi:10.1016/j.csr. 2007.09.007

Ianniello J (1977) Tidally induced residual currents in estuaries of constant breadth and depth. J Mar Res 35(4):755–786

Joyce T (1989) On in situ "calibration" of shipboard ADCPs. Journal of Atmopheric and Oceanic Technology 6:169–172

Klinck JM, O'Brien JJ, Svendsen H (1981) A simple model of fjord and coastal circulation interaction. J Phys Oceanogr 11:1612–1626

Li C, O'Donnell J (2005) The effect of channel length on the residual circulation in tidally dominated channels. J Phys Oceanogr 35: 1826–1840

Officer CB (1976) Physical oceanography of estuaries. Wiley, New York, 465 pp

Rippeth TP, Simpson JH (1998) Diurnal signals in vertical motions on the Hebridean Shelf. Limnol Oceanogr 43:1690–1696

Stigebrandt A (2012) Hydrodynamics and circulation of fjords. In: Bengtsson et al (eds) Encyclopedia of Lakes and Reservoirs. Springer, Netherlands, pp 327–244

Straneo F, Hamilton GS, Sutherland DA, Stearns LA, Davidson F, Hammil MO, Stenson GB, Rosing-Asvid A (2010) Rapid circulation of warm subtropical waters in a major, East Greenland glacial fjord. Nat Geosci 3:182–186

Stucchi DJ, Bell WH (1980) Shelf-fjord exchange on the west coast of Vancouver Island. Trans Amer Geophys Union 61:280

Svendsen H, Thompson RORY (1978) Wind-driven circulation in a fjord. J Phys Oceanogr 8:703–712

Thomson RE, Mihály SF, Kulikov EA (2007) Estuarine versus transient flow regimes in Juan de Fuca Strait. J Geophys Res 112:C09022. doi:10.1029/2006JC003925

Trump CL, Marmorino G (1997) Calibrating a gyrocompass using ADCP and DGPS data. J Atmos Ocean Technol 14:211–214

Valle-Levinson A (2008) Density-driven exchange flow in terms of the Kelvin and Ekman numbers. J Geophys Res 113:C04001. doi:10.1029/2007JC004144

Valle-Levinson A, Atkinson LP (1999) Spatial gradients in the flow over an estuarine channel. Estuaries 22(2A):179–193

Valle-Levinson A, Sarkar N, Sanay R, Soto D, León J (2007) Spatial structure of hydrography and flow in a Chilean Fjord, Estuario Reloncaví. Estuar Coasts 30(1):113–126

Valle-Levinson A, Jara F, Molinet C, Soto D (2001) Observations of intratidal variability of exchange flows cver a sill/contraction combination in a Chilean fjord. J Geophys Res 106(C4):7, 051–7,064

Winant CD (2008) Three-dimensional residual tidal circulation in an elongated, rotating basin. J Phys Oceanogr 38:1278–1295

Wong K, Valle-Levinson A (2002) On the relative importance of the remote and local wind effects on the subtidal exchange at the entrance to the Chesapeake Bay. J Mar Res 60:477–498